Available online at www.sciencedirect.com
ScienceDirect
Ultramicroscopy 107 (2007) 534–542
ultramicroscopy
www.elsevier.com/locate/ultramic

Prospects for aberration corrected electron precession

C.S. Own[a,*], W. Sinkler[b], L.D. Marks[a]

[a]Department of Materials Science and Engineering, Northwestern University, Evanston, IL 60201, USA
[b]UOP LLC, Des Plaines, IL 60017, USA

Received 16 December 2005; accepted 8 March 2006

Abstract

Recent developments in aberration control in the TEM have yielded a tremendous enhancement of direct imaging capabilities for studying atomic structures. However, aberration correction also has substantial benefits for achieving ultra-resolution in the TEM through reciprocal space techniques. Several tools are available that allow very accurate detection of the electron distribution in surfaces allowing precise atomic-scale characterization through statistical inversion techniques from diffraction data. The precession technique now appears to extend this capability to the bulk. This article covers some of the progress in this area and details requirements for a next-generation analytical diffraction instrument. An analysis of the contributions offered by aberration correction for precision electron precession is included.
© 2006 Elsevier B.V. All rights reserved.

PACS: 07.78. + s; 61.14.Dc; 61.14.Lj

Keywords: Aberration correction; Electron diffraction; Precession

1. Introduction

In many areas of microstructural characterization research one needs to know the particular phases present in a small region of a multiphasic material. One of the standard tools for this purpose is chemical characterization via EDX and/or EELS, well-established techniques. However, while these give the chemistry with a reasonable accuracy, they do not give the atomic structure. If all the possible phases present have already been determined one can compare diffraction information (e.g. spacings) against tabulated values, but this will not work for novel phases. A tool that would be very useful in many academic (and industrial) applications is the ability to directly solve the atomic structure just from local diffraction data. The instrumentation to collect such information, i.e. high-quality diffraction from regions of 1–5 nm, has existed for many years. There are also several public domain codes now available for generating structure estimates using direct methods [1,2] as well as at least one commercial package.

Unfortunately, there is a fundamental problem with the diffraction data that one obtains using conventional diffraction techniques. The intensities are dynamical, and although under certain conditions [3–5] the deviations from kinematical are not too severe, in many cases direct methods do not work and to date no algorithms have been developed that can robustly accommodate dynamical contamination. To explain briefly, direct methods are not a true mathematical inversion procedure, rather they exploit probability and statistics to find likely values for the phases based on *a priori* information. The *a priori* information can include atomicity of the scattering, positivity of the electrostatic potential and any other information. Given precise kinematical diffraction data to relatively high resolution, in almost all cases the algorithms act as a true inversion, recovering the full wave from just diffraction amplitudes. With less kinematical data they do not; some of the peaks may have the wrong positions and/or incorrect amplitudes although often this is enough to solve a structure. In pure mathematical terms (see Ref. [6] and references therein) there is no guarantee that they will always work (the problem is non-convex), and it is nearly impossible at present to predict when they will fail.

*Corresponding author.
E-mail address: csown@penelope.dhs.org (C.S. Own).

0304-3991/$ - see front matter © 2006 Elsevier B.V. All rights reserved.
doi:10.1016/j.ultramic.2006.03.011

The fundamental problem is that except for very thin samples, which project well beyond a certain thickness (about 20–30 nm) the amplitudes no longer necessarily correspond to a real-valued function in real space with peaks at the projected atom positions. In general, an integrated direct methods package like EDM will provide enough information for a structure determination, but unlike the case with X-ray diffraction this almost certainly cannot be done in a ''black-box'' fashion for all structures with conventional electron diffraction. A skilled user can solve a structure, not a novice.

The recently developed precession electron diffraction (PED) or Vincent–Midgley camera [7–15] is an interesting concept which appears to circumvent many problems with dynamical diffraction of electrons for bulk crystallographic analyses. The basic idea of such a camera is to tilt the incident electron beam in a cone about a zone axis, and simultaneously descan the beam in the final diffraction pattern (DP). The DP obtained is then an integral over a range of different directions, similar to an X-ray precession camera. It appears that direct methods work well with diffraction data from bulk crystals obtained this way [16–19], for reasons that are currently not completely understood.

We have implemented a version of the Vincent—Midgley precession camera (see Fig. 1) within our UHV-transmission electron microscope and (more recently) on a JEOL 2000FX and 3000F; to our knowledge these are the only three such cameras in the US, and there are only a handful of others in the world at present. Our approach has been to handle almost everything using software running on a conventional PC computer, so it can be rather cheaply adapted for use on any transmission microscope. Important from an experimental view, our instrument has good definition in reciprocal space including both second- and third-order aberration compensations so we can obtain accurate information from relatively large-unit cell materials. The system is very easy to use, and as far as the operator is concerned (once it has been aligned) by simply pushing a button he or she can switch from conventional small-area diffraction to precession diffraction. As part of a continuing collaboration we intend to install a camera on a new JEM-2010 at Northwestern and on a 2100F at Urbana-Champaign in the near future.

While more research needs to be done, it is already clear from the data we have that the precession approach really does eliminate many of the dynamical effects. We have looked at several different materials, and it appears that the results of a direct methods inversion are reasonably robust and accurate, see for instance Ref. [19]. Also important, we have found that we can obtain rather good quantitative agreement between experimental and precession-multislice calculated intensities (Fig. 2). While it is not possible to say that this is the ''philosopher's stone'' of electron diffraction—a general, easy to use technique for solving structures—it certainly shows great promise to be exactly this.

Analyses of simulated PED patterns have suggested that PED using higher beam tilt angles more closely approximates powder diffraction and the intensities become more kinematical with increasing cone semi-angle (ϕ) [20]. This means that larger precession semi-angle improves the ability of direct methods to find a good structure model [21]. However, optical aberrations cause defocus errors dependent on source aperture position, which manifest as radial probe shifts in the sample (image) plane. These compete with formation of a small-precessed probe, limiting the angular range. The structure itself also affects the maximum-targeted semi-angle due to first-order (FOLZ) and zoroth-order Laue zone (ZOLZ) overlap. Fig. 3(a) demonstrates this limitation: during precession the FOLZ point closest to the precession axis, defined by point F, is revolved to the opposite side of the projection axis during precession (indicated by F'). If F' lies directly

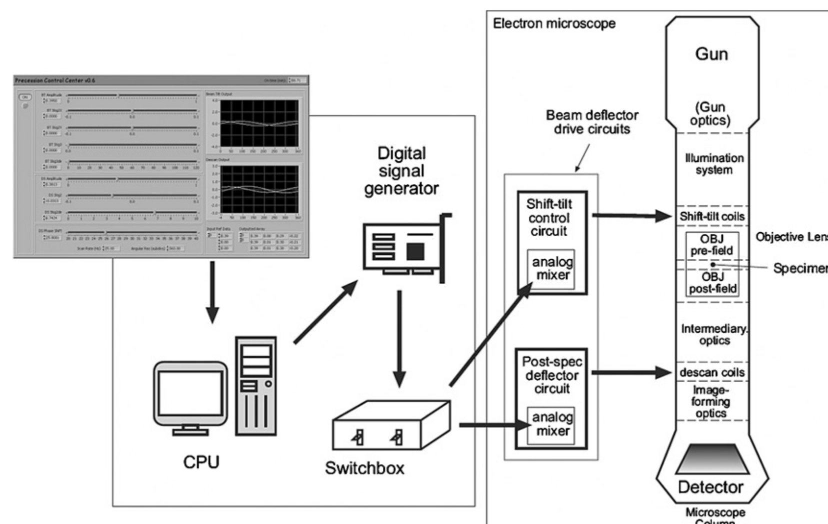

Fig. 1. Schematic diagram of the precession camera setup. A PC is used to create signals (with 2-fold and 3-fold compensations) that drive both pre-sample beam tilt and post-sample descan coils.

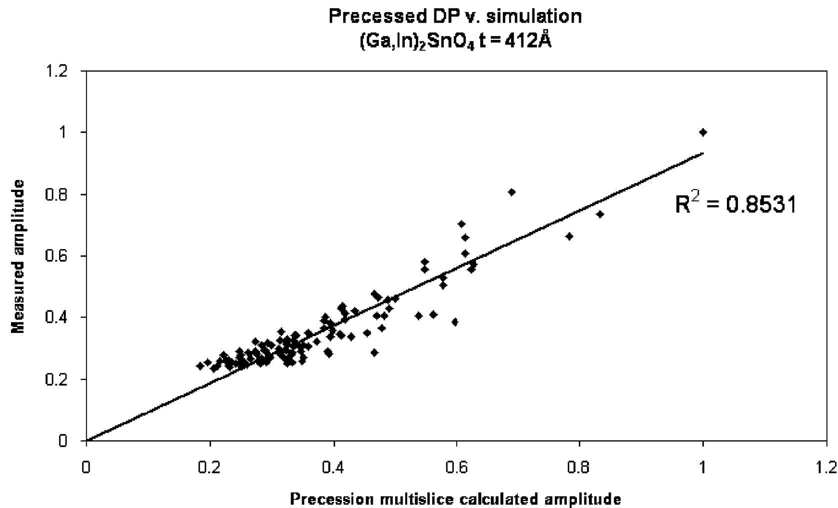

Fig. 2. Experimental precession amplitudes (normalized) plotted against amplitudes calculated by precession multislice. R_2 is the correlation coefficient. See Ref. [20] for experimental details.

above a ZOLZ reflection and has considerable scattering intensity, the zeroth-order measured intensity will be the incoherent sum of the HOLZ and ZOLZ intensities with no viable method of separating the two. This excludes structures where the HOLZ are easily distinguishable from the ZOLZ, but for unknown structures this analysis applies unequivocally. The usable radius of the DP is described by the relationship

$$\phi = \arccos\left(\frac{k\cos(\phi) - \frac{1}{c}}{k}\right) - \phi, \tag{1}$$

where ϕ is the cone semi-angle, $\boldsymbol{c}$ is the projection-axis unit cell dimension or repeat distance along the beam direction, $\boldsymbol{k}$ is the wavevector, and γ is—by the small-angle approximation—the approximate usable DP radius in radians.

Fig. 3(b) shows the unit cell dimension $\boldsymbol{c}$ plotted against γ for four different cone semi-angles, showing the rapid decrease in usable DP radius as unit cell dimension increases. For reference, $\gamma = 25\,\text{mrad}$ corresponds to $\sim 1\,\text{Å}^{-1}$ at 200 kV. Increasing ϕ also increases the Laue zone overlap constraint—in the worst case, investigating a large unit cell structure of 25 Å in the projected direction will yield very little trustworthy diffraction information when $\phi > 50\,\text{mrad}$ is used (recall that the number of reflections increases roughly with the square of $|\boldsymbol{g}|$). While it is desirable to harvest reflections to as high of resolution as possible, the most important spots for direct methods are those within an annulus containing key information about interatomic distances [22]. To generate a good initial starting structure model, direct methods should have reflections to roughly $1\,\text{Å}^{-1}$, corresponding to $\gamma \sim 25-30\,\text{mrad}$ at 200 kV. For this reason, structures or projections for which $\boldsymbol{c} > 15\,\text{Å}$ will be difficult to work with at large ϕ due to FOLZ overlap, while structures with $\boldsymbol{c} < 10\,\text{Å}$ are very amenable. Higher energy is advantageous here because the Ewald sphere is flatter for smaller λ.

PED will be most amenable for certain zones of plate-like structures, where the projection normal to the cleavage plane results in a small repeat distance along the beam direction. The $(Ga, In)_2SnO_4$ ternary oxide model system (GITO) structure is a good example: the projection-axis dimension $c = 3.17\,\text{Å}$. According to Eq. (1), GITO yields a usable DP radius (γ) of 100 mrad when $\phi = 24\,\text{mrad}$, and this decreases to about $\gamma = 60\,\text{mrad}$ (quite ample) when $\phi = 100\,\text{mrad}$. It should be noted that the ZOLZ reflections can potentially be recovered if a partial scan ($\theta = [0, \pi]$ radians) is used. The logical extension of this is a data-mining approach where discrete tilts are acquired independently and the spots integrated in software rather than within a single exposure. This approach is rather complex in terms of implementation but very powerful, since the residual dynamical behavior may be characterizable and possibly removed for individual tilts.

At present the primary instrumental limitation is keeping the illuminated area small while tilting by relatively large angles. For an ideal instrument, we can estimate that the requirements will be:

- Probe size 1–2 nm—Koehler illumination.
- Probe displacement $< 5\%$ at a tilt of 75 mrad, for applicability to nanocrystalline phases.
- Probe distortions $< 5\%$ at a tilt of 75 mrad.
- Minimal projector distortions (otherwise there can be severe quantitation problems).
- Energy filtering for plasmons.[1]
- Low temperature (to reduce phonon scattering).
- Adequate detectors (need 10^5–10^6 counts/pixel without damage).

[1] While Jansen et al. [23] reported that energy filtering with parallel illumination did not improve refinements for samples to 25 nm, PED is useful for thicker specimens (50 + nm), where inelastic scattering is considerable.

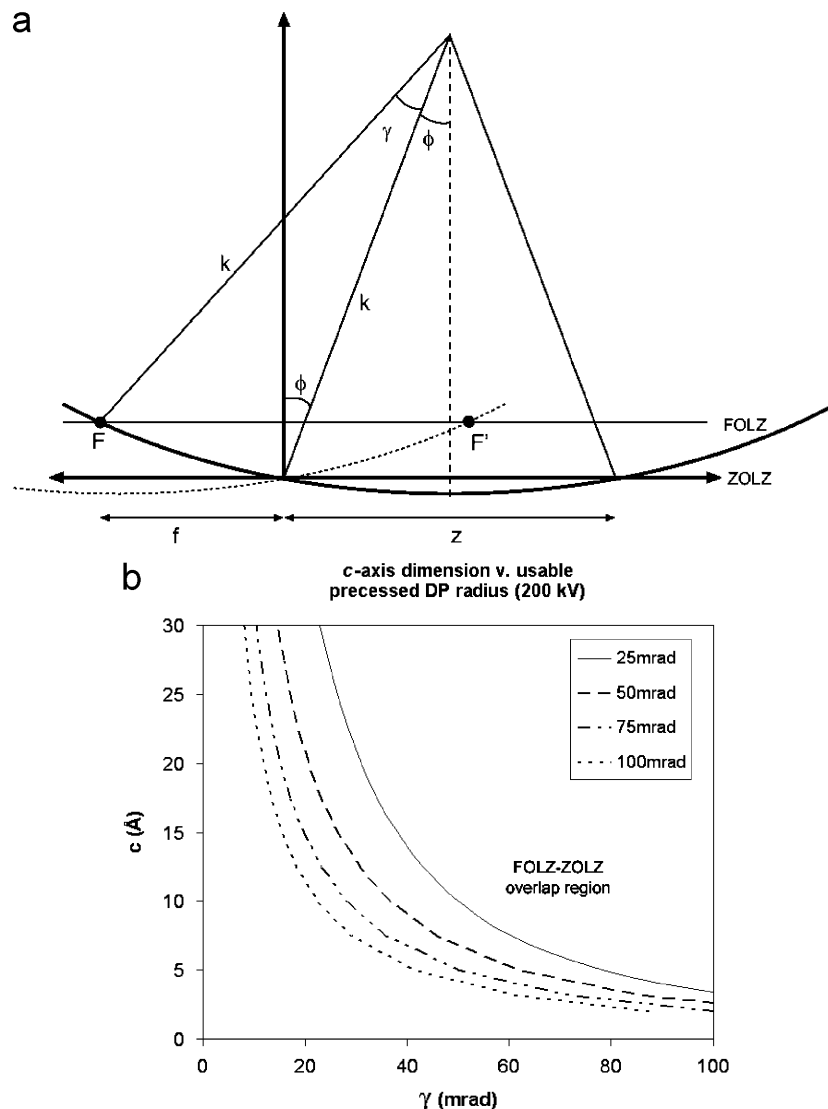

Fig. 3. (a) Precession geometry schematic showing the relationship between ZOLZ and FOLZ excitations. The distance z corresponds to the zero order zone radius; γ corresponds to the usable diffraction radius in mrad. (b) Plot of unit-cell dimension against usable diffraction radius γ for various cone semi-angles. The lines describe γ, which decreases with ϕ and specimen unit-cell thickness.

- Very fast detector data capture rates (for software-based integration in the event that Laue zone overlap prevents acquisition).
- Stable sample tilting through reasonable angles (±30 mrad or more).

No current instrument can do this, although some of the C_s corrected instruments being built may approach this. The intention of this article is to consider how one might be able to achieve these goals using an aberration corrected instrument.

2. Aberration analysis

Electron precession has been shown to be easily retro-fitted onto conventional instruments, effectively extending the ultimate resolution of such instruments for the study of bulk structures. While the precession mode can be implemented on a variety of instruments, ultimate performance is still limited by the classic problem of objective lens (OL) aberrations. The primary difficulty in implementing electron precession on conventional instruments lies in the objective's ability to accurately focus high-angle rays onto a small region of the specimen, and to release the diffracted beams in trajectories that correctly describe the diffraction vectors with respect to the incident radiation. Aberrations throughout the optical system adversely affect the ray trajectories, resulting in a delocalized hollow cone probe fulcrum at the specimen and poorly converging diffraction points at the diffraction plane.

Fig. 4 is a schematic of a modern condenser-objective instrument showing the ray paths traversed by a precessed transmitted beam as it passes through the specimen. It demonstrates in more detail the role of the OL in PED. The convergence point at the specimen should ideally be as small as possible to reduce the chance of illuminating

a specimen defect and to minimize the variation in sample thickness and orientation. Aberrations are inherent in all cylindrically symmetric round lenses [24], therefore, the ray path of the incident beam will necessarily deviate from ideal as the incident beam precesses azimuthally through the OL field. This may cause the probe to wander in the image (specimen) plane during precession. Highest performance is obtained when the alignment is optimized to minimize this wandering effect.

An idea of minimum probe size that can be obtained is available by studying the behavior of convergent probes. In conventional microdiffraction, the diameter d (containing 70% of the intensity) of a filled convergent probe is dominated by the spherical aberration coefficient C_s, and is described by the following relation:

$$d_{70\%} = 0.66\lambda^{3/4}C_s^{1/4}, \tag{2}$$

where λ is the electron wavelength [25]. In Eq. (2), the defocus has been optimized to yield the smallest probe. This puts strict constraints upon precession: the smallest probe size is obtained when C_s is minimized and when the defocus term is smaller than the spherical aberration term. Minimum C_s is obtained at a specific known lens excitation (in amperes) that is optimized by the manufacturer for the column and different for every lens. Therefore, to obtain the finest probe, the defocus must be tuned not by the OL excitation, which is fixed, but by the specimen height z (i.e., it must be tuned mechanically). At the start of alignment, the specimen must therefore be at the eucentric height ($\Delta z = 0$), which is usually the expected crossover.[2] The unaligned condition yields a circle only if non-spherical aberration terms are small (as indicated in Figs. 4 and 5); ellipses or polygons/stars result if the non-spherical terms are large. Fig. 5 shows a case where the threefold aberration is prominent. After alignment, the lobes in the image were brought down to a disc approximately 25 nm in diameter.

PED involves much larger angles than the conventional probe convergence angle of micro- and nano-diffraction, hence higher order aberrations and their effects should be considered.[3] The aberration function is described by radial and axial components in the $x-y$ plane in the Krivanek notation, a convenient form for precession [26]. The following aberration function is expanded to fourth order in this notation:

$$\begin{aligned}\chi(\rho,\theta) = {} & \rho(C_{01a}\cos(\theta) + C_{01b}\sin(\theta)) \\ & + \frac{\rho^2}{2}(C_{10} + C_{12a}\cos(2\theta) + C_{12b}\sin(2\theta)) \\ & + \frac{\rho^3}{3}(C_{23a}\cos(3\theta) + C_{23b}\sin(3\theta) \\ & + C_{21a}\cos(\theta) + C_{21b}\sin(\theta)) \\ & + \frac{\rho^4}{4}(C_{30} + C_{34a}\cos(4\theta) + C_{34b}\sin(4\theta) \\ & + C_{32a}\cos(2\theta) + C_{32b}\sin(2\theta)) \\ & + \frac{\rho^3}{3}(C_{45a}\cos(5\theta) + C_{45b}\sin(5\theta) + C_{43a}\cos(3\theta) \\ & + C_{43b}\sin(3\theta) + C_{41a}\cos(\theta) + C_{41b}\sin(\theta)).\end{aligned} \tag{3}$$

[2] Eucentric height is formally defined as the height of the specimen at which its image does not move laterally as a function of specimen tilt.

[3] This discussion excludes diffraction ronchigrams, which are often used for probing and tuning aberrations in aberration-corrective systems. The convergence angle in ronchigrams is often hundreds of mrad.

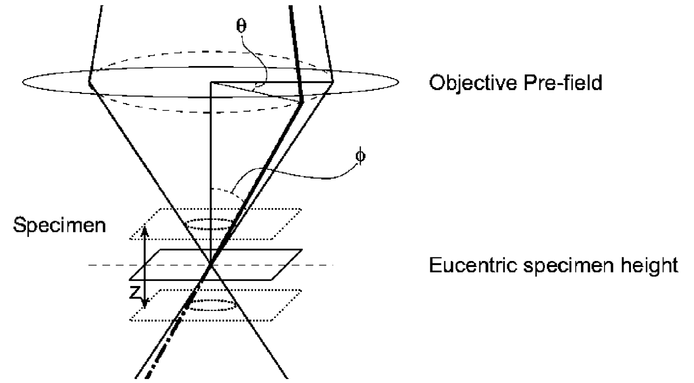

Fig. 4. Precession geometry near the OL in a modern condenser-objective TEM with double deflection coil system showing the path of the precessed transmitted beam.

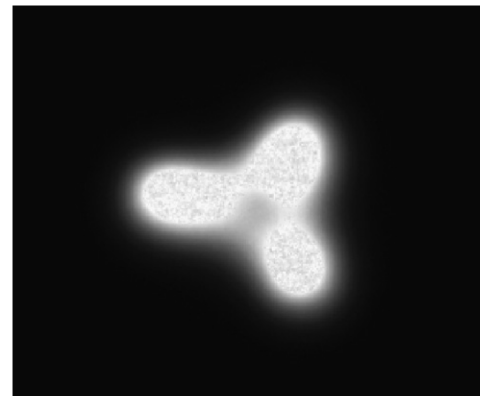

Fig. 5. Star of merced, formed by the unoptimized precession probe prior to full alignment. The threefold astigmatism term is dominant. Each lobe is roughly 25 nm. The image was taken on a JEOL 2000FX retrofitted for precession.

χ describes the distance between the aberrated wavefront and the Gaussian wavefront along the aberrated ray (see Fig. 6); a ray intersecting the aberration function at a point (ρ, θ) will be subjected to a deviation described by a polynomial radially and a harmonic function azimuthally. For precession, we are interested in illuminating the lens in an annulus whose radius is considerably beyond the limits of conventional TEM imaging. The minimum desired ϕ is on the order of 20 mrad, and benefits continue to occur past 50 mrad. In real space, the aberration function produces a deviation from the Gaussian focal point (wandering probe), and in reciprocal space, a deviation in the ray's incidence angle. In practice either is easy to optimize by itself; however, correcting one

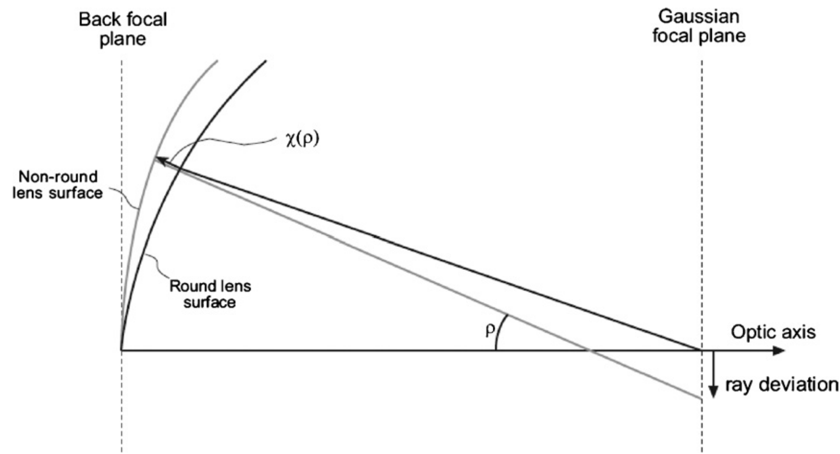

Fig. 6. The aberration function $\chi(\rho)$ describes the deviation from the ideal round lens along the projected direction of the aberrated ray. The aberrated ray deviates in angle from ideal by ρ; in real space this corresponds to a deviation of probe location (the origin of probe 'wandering').

without compromising the other is the major challenge in aligning a precession system. Consistency of the cone semi-angle has proven to be a relatively loose constraint (± 1 mrad is sufficient, see Ref. [15]) so real space localization can be considered the primary optimization constraint.

It has already been mentioned that spherical aberration can be roughly compensated by a simple defocus adjustment or more preferably by a shift in specimen height to preserve optimal excitation of the objective. In conventional microscopes, the next limiting aberration after C_s is a threefold astigmatism [27]. Twofold is present but can be corrected by the objective stigmators. The coefficients of largest concern in the context of Eq. (3) are three-fold astigmatism (C_{23a} and C_{23b}) and twofold astigmatism (C_{12a} and C_{12b}), illustrated in Fig. 7.

Beam tilt purity and the twofold OL stigmators can compensate for most of C_{12}, however, sometimes C_{23} is left over and must be corrected dynamically during scan alignment. In our precession implementations, additional twofold and threefold compensations are made in the conical scan in conjunction with tilt purity adjustments to achieve a suitable compromise between incident ray direction in reciprocal space and real space convergence. The practical limits have been about 40–50 mrad in the JEOL instrument. Above this threshold we have found a combination of higher-order objective aberrations and projector distortions to dominate. The present figures assume parallel illumination; assuming an aberration-free imaging system, at high angles a beam with finite convergence yields spots with differing shapes which may complicate data collection.

Aberration-corrected instruments are particularly suitable for the precession mode. Scan systems with several degrees of freedom are by default incorporated into the latest instruments and are well suited for providing the deflections for conical illumination. The latest generation correctors can provide up to about 70 mrad cone semi-angle without geometric compensation in the scan, thus a simple circular deflection path will automatically yield optimal conditions for the experiment. Especially advantageous is the fact that experiments can be executed at various ϕ with single-variable adjustment allowing quick experiment setup and enabling non-conical experimental geometries (potentially useful as alternative modes of precession) that would otherwise be impossible to generate without a comprehensive aberration model of the microscope column.

In such instruments the primary aberrations are of higher-order. Beyond the flat phase patch, the aberration function increases rapidly (e.g., correction to C_5 in the latest Nion Co. corrector produces an aberration function increasing to the 6th power with angle). An attempt to extend the precession semi-angle to very high values (>75 mrad) will yield rapidly diminishing returns. However, geometric compensation similar to that used on the Northwestern implementations utilizing an N-fold function, where $N-1$ is the corrector order, should nevertheless yield beneficial results.

The de-scan section of the precession instrument collects diffracted beams from each tilt condition into discrete integrated spots suitable for quantitation. This collection must happen somewhere between the image plane and back focal plane. The constraints differ from the beam tilt because the symmetry about the specimen between illumination and image forming optics is broken (except in the case where immediately post-specimen deflectors are available). Since precession involves angles considerably larger than those in conventional DPs, and the physical size of the pattern becomes larger as the diffracted beams travel from the specimen toward the detector, de-scan deflectors must be able to provide larger deflection angles. The large distance from the optic axis also subjects the diffracted beams to distortion in the intermediary lenses (astigmatism) and projector lens distortion (astigmatism, pincushion/barrel, and spiral).

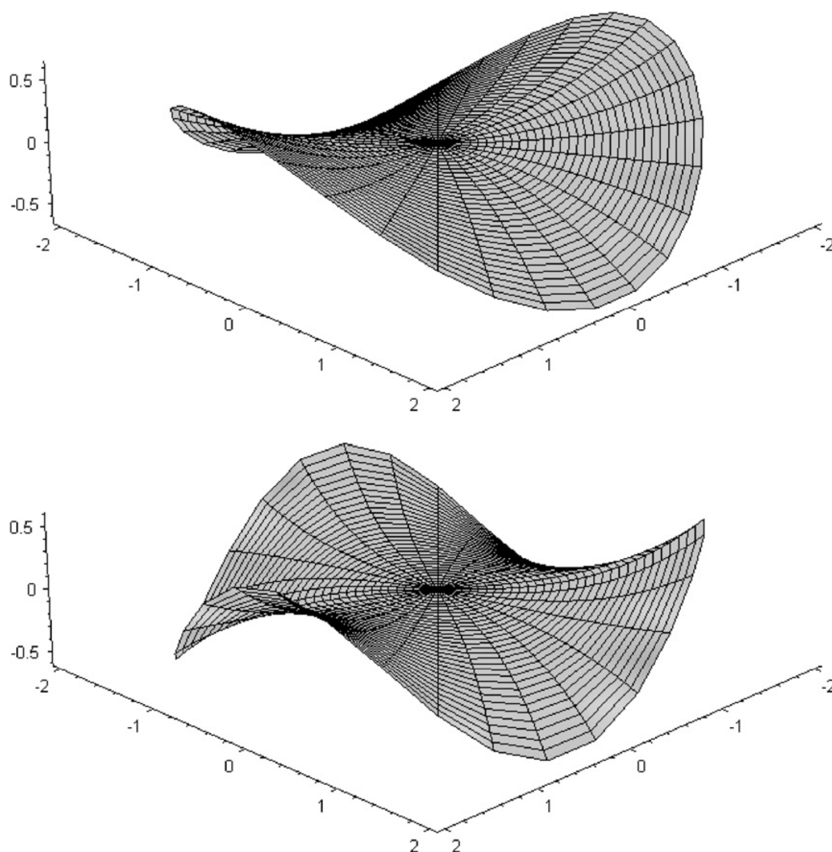

Fig. 7. (a) Twofold (potato chip) and (b) threefold (monkey's saddle) aberration functions (arbitrary units). These are the primary aberrations that require compensation in conventional instruments.

The de-scan should ideally be executed as close to the specimen as possible to minimize these effects. The second choice is in the intermediary optics, where the beam is still small. Sometimes this is not possible because the intermediate alignment deflectors are too feeble. The last resort is the imaging deflector: almost all conventional instruments incorporate a user-accessible deflector located just prior to the projector lens along the optical path. Newer instruments are incorporating more post-specimen deflection coils, therefore, better de-scan may be achieved in modern instruments.

The ability to tailor the aberrated wavefront extends naturally to an ultra-high-angle dynamically correcting scheme, suggested by N. Dellby of Nion Co. Since the precession is executed in discrete steps and the incident beam typically has small convergence (<5 mrad), the correction system can extend the hollow probe performance in a given angular direction by compromising the central disc of flat phase and shifting it off of the lens axis. The aberration function of Fig. 8 demonstrates this principle.

The aberration function displayed contains a mixture of C_{10}, C_{12a}, C_{30} (or C_s), and C_{45a} to create an extended flat phase patch that could in practice be scanned around the lens axis by altering the aberration coefficients dynamically. Similarly, a rotationally symmetric ridge function (muffin tin form) could be generated—effectively a combination of defocus, C_s, and C_5—creating a flat phase annulus that, while not focusing central rays to the Gaussian plane, is nevertheless suitable for high-angle conical precession. This would extend the usable convergence semi-angle to beyond 75 mrad while maintaining a static set of aberration coefficients, yielding excellent stability and higher angles than those achievable with an instrument corrected for zero C_s.

3. Discussion and conclusions

The analysis that we have presented indicates that, at least in principle, it should be possible to remove the primary instrumental limitations on precession diffraction due to the OL aberrations by using a dynamic approach to the aberration correction. There are two important caveats:

(1) We have ignored completely any aberrations in the lower parts of the column, which can be an issue when one wants highly accurate intensity measurements. The most accurate method we know of for measuring the intensities is a cross-correlation approach against an average diffraction spot profile, since this eliminates issues with shape-function effects due to finite objects

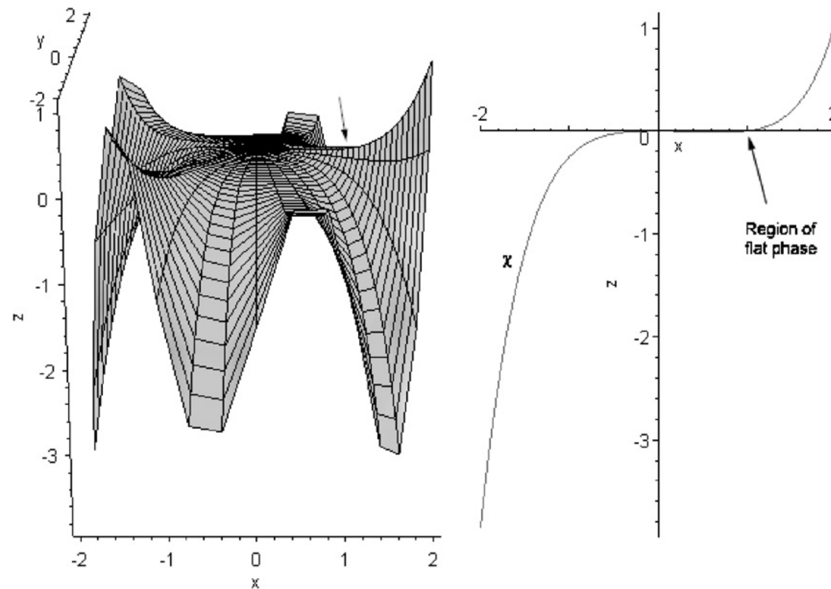

Fig. 8. An aberration function containing coefficients C_{10}, C_{12a}, C_{30}, and C_{45a} (mixed in a respective ratio of 1:2:3:3). The effective aberration surface has rough 5-fold symmetry. In the $x-z$ section on the right, an odd-order function describes a region of flat phase extended in the $+x$ direction indicated by the arrows.

and/or illuminated regions. If there are aberrations further along the optic path, particularly in the descanning of the illumination, the profiles are no longer identical. In this case the only approach is to integrate the intensity over some region, then perform some type of background subtraction; the latter will inevitably introduce some errors.

(2) It is highly desirable to be able to energy filter the diffraction data, primarily to remove the inelastically scattered low-loss electrons (energy losses of 2 eV or higher) that are problematic in thicker specimens where the precession diffraction would be most useful. Obtaining adequate energy filtering at large tilt angles may be an issue, and we have not addressed this here. Additionally, attempts so far at inverting precession data from very thick specimens (>70 nm) have met with varied success so this caveat may only become relevant as the technique matures.

Apart from the caveats above, we have detailed in this paper some of the instrumental barriers preventing higher performance in precession electron diffraction, and have suggested solutions based upon the use of corrective optics. While the primary focus on electron optical aberration correction since its realization has been on the unprecedented direct imaging performance, it is pointed out here that aberration correction has much to offer to electron diffraction technique as well. By increasing the range of obtainable illumination cone semi-angles and/or improving probe localization, precession diffraction becomes much more effective. Used in tandem with direct imaging, diffraction can further improve the atomic-scale information available in the TEM, because diffraction data contain much higher spatial frequencies and are not as sensitive to system instabilities, image resolution can be readily enhanced through phase extension techniques. Additionally, aberration-corrected precession machines will also be inherently equipped for nanoprobe hollow cone illumination, a boon to imaging applications that can make use of this (such as tomography where diffraction effects complicate 3D reconstruction and can be removed by rocking the illumination).

There is still considerable work to be done in order to validate precession diffraction as a stand-alone characterization method. However, in the process to understand the physics and to improve it, research in precession diffraction has revealed some machine limitations that, if overcome, would dramatically improve the abilities of an ultra-high-resolution analytical diffraction HREM or STEM instrument. The burden is on microscope manufacturers to produce the machines that can meet the new performance requirements for future work in this area. Of particular note is the ability to use a computer-controlled microscope to capture individual DPs from discrete tilts and then integrate their intensities in software, as detailed earlier in the paper. Computer automation is also critical for running correctors and therefore lends itself directly to controlling the conical illumination system with great precision. The variety of technologies for creating such a machine are readily accessible, and only need merging into a monolithic system to enable extraction of an enhanced level of atomic-scale information from specimens in the TEM.

Acknowledgments

Funding for this work was provided by the US Department of Energy (Grant no. DE-FG02-03ER 15457) and the Fannie and John Hertz Foundation.

References

[1] J. Jansen, D. Tang, H. Zandbergen, H. Schenk, Acta Crystallogr. Sect. A 54 (1998) 91.
[2] R. Kilaas, L. Marks, C. Own, Ultramicroscopy 102 (2005) 233.
[3] J. Hu, F. Chukhovskii, L. Marks, Acta Crystallogr. Sect. A 56 (2000) 458.
[4] F. Chukhovskii, J. Hu, L. Marks, Acta Crystallogr. Sect. A 57 (2001) 231.
[5] L. Marks, W. Sinkler, Microsc. Microanal. 9 (2003) 399.
[6] L. Marks, W. Sinkler, E. Landree, Acta Crystallogr. Sect. A 55 (1999) 601.
[7] R. Vincent, P. Midgley, Ultramicroscopy 53 (1994) 271.
[8] K. Gjønnes, Ultramicroscopy 69 (1997) 1.
[9] K. Gjønnes, Y. Cheng, B. Berg, V. Hansen, Acta Crystallogr. Sect. A 54 (1998) 102.
[10] B. Berg, V. Hansen, P. Midgley, J. Gjønnes, Ultramicroscopy 74 (1998) 147.
[11] P. Midgley, M. Sleight, M. Saunders, R. Vincent, Ultramicroscopy 75 (1998) 61.
[12] M. Gemmi, Precession technique, in: J. Puiggali, A. Rodriquez-Galan, L. Franco, M. Casas (Eds.), Electron Crystallography and Cryo-Electron Microscopy on Inorganic Materials and Organic and Biological Molecules, Universitat Politecnica De Catalunya, Barcelona, 2001, pp. L91–L97.
[13] C. Own, A. Subramanian, L. Marks, Microsc. Microanal. 10 (2004) 96.
[14] C. Own, L. Marks, Hollow-cone electron diffraction system. US Patent application no: 60/531,641.
[15] C. Own, L. Marks, W. Sinkler, Rev. Sci. Instrum. 76 (2005) (Article no. 033703).
[16] J. Gjønnes, V. Hansen, B. Berg, P. Runde, Y. Cheng, K. Gjønnes, D. Dorset, C. Gilmore, Acta Crystallogr. Sect. A 54 (1998) 306.
[17] M. Gemmi, X. Zou, S. Hovmoller, A. Migliori, M. Vennstrom, Y. Andersson, Acta Crystallogr. Sect. A 59 (2003) 117.
[18] J. Gjønnes, V. Hansen, A. Kverneland, Microsc. Microanal. 10 (2004) 16.
[19] C. Own, L. Marks, Ultramicroscopy 106 (2006) 114.
[20] C. Own, W. Sinkler, L. Marks, Acta Crystallogr. Sect. A 62 (2006) 434.
[21] C. Own, System Design and Verification of the Precession Electron Diffraction Technique, Northwestern University, Chicago, 2005.
[22] W. Sinkler, L. Marks, D. Edwards, T. Mason, K. Poeppelmeier, Z. Hu, J. Jorgensen, J. Solid State Chem. 136 (1998) 145.
[23] J. Jansen, J. Jansen, H.W. Zandbergen, M.T. Otten, Ultramicroscopy 98 (2004) 165.
[24] O. Scherzer, Z. Phys. 101 (1936) 593.
[25] J. Spence, J. Zuo, Electron Microdiffraction, Plenum Press, New York, 1992.
[26] O. Krivanek, N. Dellby, A. Lupini, Ultramicroscopy 78 (1999) 1.
[27] O. Krivanek, P. Stadelmann, Ultramicroscopy 60 (1995) 103.